European Journal of Medicinal Chemistry 301 (2026) 118216

Contents lists available at ScienceDirect

European Journal of Medicinal Chemistry

journal homepage: www.elsevier.com/locate/ejmech

Research paper

Repurposing carboplatin-based Pt(IV)-deferoxamine conjugates for infection theranostics

Martin Kraihammer [a], Hristo P. Varbanov [b,c], Kateřina Dvořáková Bendová [d], Miloš Petřík [d,e,f], Annie Yap [g], Giacomo Gariglio [a], Hubertus Haas [g,*], Clemens Decristoforo [a,**]

[a] Department of Nuclear Medicine, Medical University Innsbruck, Innsbruck, Austria
[b] Department of Pharmaceutical Chemistry, Institute of Pharmacy, University of Innsbruck, Innsbruck, Austria
[c] Department of Pharmaceutical Sciences, Medical College, Trakia University-Stara Zagora, Stara Zagora, Bulgaria
[d] Institute of Molecular and Translational Medicine, Faculty of Medicine and Dentistry, Palacký University, Olomouc, Czech Republic
[e] Czech Advanced Technology and Research Institute, Palacký University, Olomouc, Czech Republic
[f] University Hospital Olomouc, Olomouc, Czech Republic
[g] Institute of Molecular Biology, Biocenter, Medical University Innsbruck, Innsbruck, Austria

ARTICLE INFO

Keywords:
Carboplatin
Pt(IV) complexes
Deferoxamine
PET
Gallium-68
Infection imaging
Aspergillus fumigatus
Fungal theranostics

ABSTRACT

Recently, multifunctional platinum(IV) complexes designed as prodrugs for the anticancer drug carboplatin and the iron chelator deferoxamine (DFO), each featuring a DFO unit at one axial position and either hemisuccinate or acetate at the other, were developed. As these compounds contain DFO, they hold the potential to be radiolabelled with gallium-68 for molecular imaging and to be recognized by microorganisms, which can utilise DFO as a siderophore-based iron source being taken up by specific siderophore transporters (SITs). Combining this recognition mechanism with a cytotoxic carboplatin core, these compounds could potentially lead to specific antimicrobial activity, particularly against *Aspergillus fumigatus* (AFU), which causes systemic infections and expresses relevant SITs. The two complexes were radiolabelled with gallium-68 and evaluated for radiochemical purity and protein binding, exhibiting quantitative ^{68}Ga-labeling yields with high radiochemical purity and stability in human serum as well as low protein binding. *In vitro* uptake assays in AFU and AFU mutants lacking SITs were performed as well as MIC assays for assessment of antifungal activity in comparison to DFO and carboplatin alone. Complexes were also evaluated in *in vivo* assays including stability studies in healthy mice as well as biodistribution studies and PET imaging in a rat pulmonary aspergillosis model, revealing favourable pharmacokinetics with rapid distribution and a renal excretion pattern with pronounced accumulation in AFU infected lung tissue. However, rapid metabolism of the complexes was observed already 5 min p.i. in serum and urine samples. Overall, this study demonstrates the potential of carboplatin-based Pt(IV)-DFO conjugates for application in infection theranostics.

1. Introduction

Recently observed synergistic interactions between the anticancer drug carboplatin and the iron chelator deferoxamine (DFO) (Fig. 1a and b) in A549 (human non-small cell lung cancer) cells [1] have inspired the development of multifunctional platinum(IV) complexes designed as prodrugs for co-delivery of both agents. Structurally, these Pt(IV) compounds retain the equatorial coordination sphere of carboplatin, with one or two DFO units attached to the axial ligands via succinate linkers (Fig. 1, c). These complexes exhibited only moderate *in vitro* cytotoxicity, with IC_{50} values generally exceeding those of carboplatin in the tested cell culture models (15–26 times higher in CH1/PA-1 (ovarian teratocarcinoma), 2–6 times higher in SW480 (colon carcinoma), and 1–8 times higher in A549), likely due to limited uptake in the cancer cells and/or slow rate of intracellular activation [2].

Nonetheless, the favourable physicochemical properties of the complexes, along with the preserved chelating ability of the DFO moiety conjugated to the Pt(IV) core make them promising candidates for theranostic applications. Supporting this potential, Sadler et al. have recently synthesized a photoactivatable diazido Pt(IV) complex with a

* Corresponding author.
** Corresponding author.
E-mail addresses: hubertus.haas@i-med.ac.at (H. Haas), clemens.decristoforo@i-med.ac.at (C. Decristoforo).

https://doi.org/10.1016/j.ejmech.2025.118216
Received 18 June 2025; Received in revised form 25 September 2025; Accepted 26 September 2025
Available online 26 September 2025

DFO unit attached at axial position (Fig. 1, d) and measured its biodistribution in mice by dynamic Positron Emission Tomography (PET) imaging after radiolabelling with gallium-68 [3], a short lived positron emitter available from ^{68}Ge/^{68}Ga radionuclide generators.

Moreover, Pt(IV)-DFO conjugates represent interesting candidates for antimicrobial agents with the potential to selectively target pathogenic bacteria and fungi, that take up Fe(III) and Ga(III) complexes of DFO through specific siderophore transporters (SITs). Proof of this concept has already been established for DFO labelled with gallium-68, which demonstrated promising results in bacterial infections [4]. Utilising DFO as a carrier of metallodrugs has already been reported by Dyson et al. in attempt to develop new ruthenium-based antibacterial agents [5]. Apart from bacterial infections, ^{68}Ga-labelled DFO also exhibits high and specific accumulation in fungal infections with *Aspergillus fumigatus* (AFU) [6]. This mold species is of great clinical importance as it causes pulmonary aspergillosis in humans, a life-threatening form of fungal infection, primarily in immunocompromised patients. This pathology is associated with significant morbidity and mortality due to limitations both in diagnosis [7] and treatment [8]. Standard diagnostic procedures for pulmonary aspergillosis include culturing from biological samples, requiring invasive measures to collect the samples and sufficient time to grow the cultures, as well as non-specific imaging techniques like CT or MRI, which cannot differentiate between fungal infections and radiologically similar pathologies [8,9]. Current treatment options for aspergillosis include triazole antifungal agents i.e. itraconazole, liposomal amphotericin B and echinocandins i.e. caspofungin [8,10].

Our group has studied the use of siderophores labelled with gallium-68 for PET imaging of infections, exploring various approaches [11]. The specific recognition by microbes via specific SITs, upregulated in the infection setting make them a promising approach to target infections. We have used the siderophore system for a variety of applications including infection theranostics in fungal as well as bacterial infections. Two clinical trials focused on infection imaging utilising siderophores radiolabelled with gallium-68 in humans are currently ongoing [12,13]. Recently, we studied a series of conjugates of small antifungal molecules with triacetylfusarinine C (TAFC), a fungal specific siderophore, for imaging and treatment of invasive aspergillosis. This provided a proof of concept [14], however with limited *in vitro* activity amounting to MIC values not exceeding 16 μg/mL. The two Pt(IV)-DFO-conjugates included in this study were originally designed as anticancer drugs. However, the combination of a cytotoxic Pt(IV) carboplatin derivative with a microbe-specific targeting group in the form of DFO, which can coordinate gallium-68 for PET imaging, raised our interest. Likewise, labelling with stable gallium for recognition by fungal SITs could allow evaluation of the potential of the compounds for an antifungal "theranostic" approach. We recently could show that ferrioxamines are specifically taken up by AFU by the Sit1 transporter [15]. To further investigate this, we developed specific mutants lacking or overexpressing this target, allowing mechanistic investigations of the utilization of therapeutic siderophore conjugates, which was utilized in this study. Interestingly, uptake efficiency by AFU of [^{68}Ga]Ga-DFO was pH dependent and could be improved by acetylation of DFO, resulting in an uncharged gallium complex.

Apart from imaging application via PET, utilising the DFO/siderophore transporter system for drug targeting, could enable the Pt(IV)-DFO complex to be delivered directly to microbial pathogens, where it will be activated upon reduction to the cytotoxic Pt(II) species. Thus, this complex holds the potential to be used as a novel theranostic agent in fungal infections, possibly circumventing the low cytotoxic effects observed in cancer cell lines. Moreover, antineoplastic platinum-based drugs exhibit a broad antimicrobial spectrum of activity, including efficacy against multi-drug resistant pathogens [16,17].

In this study we radiolabelled two carboplatin-based Pt(IV)-DFO conjugates, each featuring a DFO unit at one axial position and either an acetate or hemisuccinate at the other (Fig. 2) with gallium-68 for Positron Emission Tomography (PET). We report on their *in vitro* and *in vivo* properties with respect to repurposing these compounds for theranostics in fungal infections with AFU, which has shown strong and selective accumulation of [^{68}Ga]Ga-DFO *in vivo* [6].

2. Results

2.1. Radiolabelling

Radiolabelling of all compounds was achieved with almost quantitative radiochemical yields by incubation for 10 min at room temperature as analysed by ITLC, without detection of unbound gallium-68 species. Even though chemical purity of the compounds **1** and **2** was >95 %, a pre-peak with a relative retention to the main ^{68}Ga-labelled conjugate of about 0.9 was observed in the radiochromatograms for both conjugates **1a** and **2a**. This pre-peak accounted for approximately 6 % and 12 % of that of the main ^{68}Ga-labelled conjugate signal for **1a** and **2a**, respectively. Radiolabelling of DFO-succinate resulted in a peak with corresponding retention time to this pre-peak. As unbound gallium-68 was detected neither by HPLC nor TLC the radiolabelling, solutions were used without further purification. The supplementary material contains sample chromatograms for TLC (Fig. S1 for [^{68}Ga]Ga-conjugate **1a**, Fig. S2 for [^{68}Ga]Ga-conjugate **2a**), UV trace (Fig. S3) and radiotrace (Fig. S4) of RP-HPLC as well as ESI-MS (Fig. S5).

2.2. Serum stability and protein binding

Stability studies in aqueous solution and in human serum indicated no change of composition in radio-HPLC analysis as shown in Fig. 3. For both conditions, the main impurity observed was a chemical species

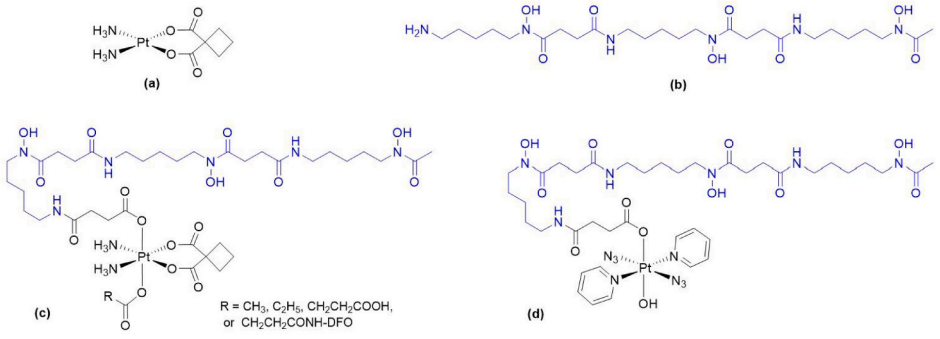

Fig. 1. Chemical structures of (a) carboplatin, (b) deferoxamine, (c) carboplatin-based Pt(IV)-DFO prodrugs [2], and (d) a photoactivatable diazido Pt(IV)-DFO complex [3].

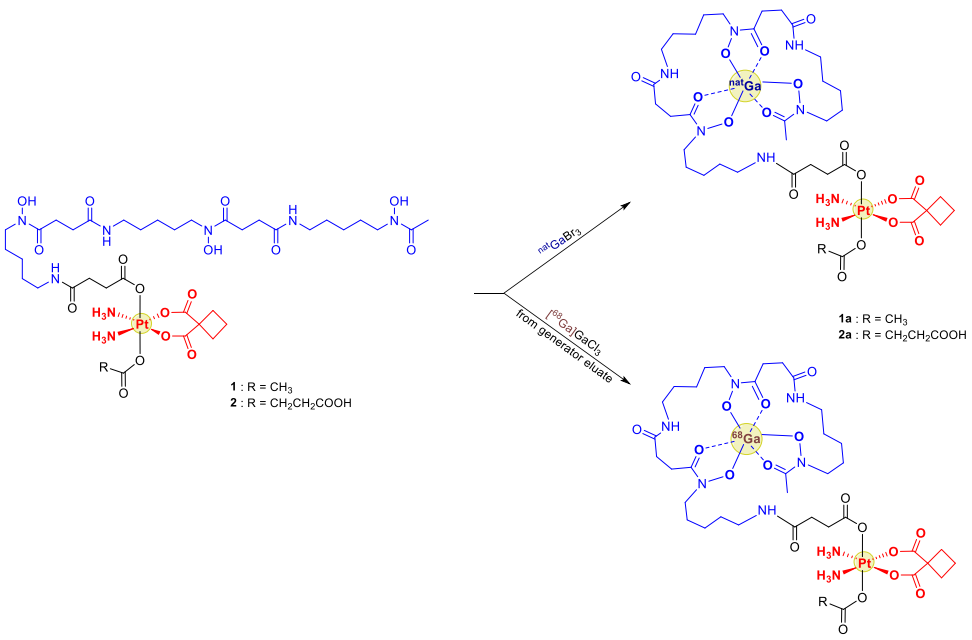

Fig. 2. Reaction of previously published [2] Pt(IV)-DFO conjugates **1** and **2** with either [^{nat}Ga]$GaBr_3$ or [^{68}Ga]$GaCl_3$ to the respective heterobimetallic complexes **1a** and **2a**. ^{nat}Ga-conjugates **1a** and **2a** were only used as non-radioactive counterparts to perform MIC assays.

with retention time corresponding to [^{68}Ga]Ga-DFO-succinate. For serum stability testing, conjugate **1a** showed >92 % intact compound for all time points, which corresponds to the radiochemical purity after radiolabelling. 92.2 % conjugate **1a** was found intact after 15 min of incubation in human serum, 92.7 % after 30 min and 93.9 % after 60 min. Radiochemical purity after radiolabelling was overall lower for conjugate **2a** and was >84 % for all time points during serum stability testing: 86.3 % intact compound was found after 15 min of incubation, 84.8 % after 30 min and 86.8 % after 60 min. Also, when incubating in kidney or liver homogenates no degradation of the main peak could be detected indicating high *in vitro* stability of the ^{68}Ga-labelled conjugates.

Protein binding tests showed protein bound fractions of <11 % for both compounds. Protein-bound fraction for conjugate **1a** was 9.5 ± 0.7 % after 15 min, 9.6 ± 0.6 % after 30 min and 9.4 ± 1.3 % after 60 min (values given as means ± SD with n = 2). Conjugate **2a** showed overall lower protein-binding properties with 4.3 ± 0.2 % after 15 min, 3.8 ± 0.3 % after 30 min and 4.7 ± 0.1 % after 60 min (values given as means ± SD with n = 2).

2.3. Conjugate stability in female BALB/c mice and in AFU cultures

Fig. 3 shows HPLC radiochromatograms of samples for both ^{68}Ga-labelled conjugates under different *in vitro* and *in vivo* conditions with mixtures of [^{68}Ga]Ga-DFO, [^{68}Ga]Ga-DFO-succinate and either [^{68}Ga]Ga-conjugate **1a** or **2a** as reference. Even though both compounds were stable in human serum *in vitro*, rapid metabolism was seen *in vivo* at different time points after injection in mice, forming a main metabolite with a relative retention of about 0.9 compared to the intact conjugates. [^{68}Ga]Ga-conjugate **2a** showed slightly lower stability than [^{68}Ga]Ga-conjugate **1a** when comparing measurements from mouse serum after 5 min and mouse urine after 15 min. The retention time of this metabolite matched the retention time of [^{68}Ga]Ga-DFO-succinate, indicating its release from the Pt(IV) complexes *in vivo* by hydrolysis or reductive elimination. 15 min after injection, only the main metabolite and no intact compound could be detected in serum. The same metabolite was also identified in urine samples, along with the parent compounds and other degradation products. *In vitro* stability tests with AFU cultures showed intact ^{68}Ga-labelled conjugates for both compounds, but also degradation inside of the fungal cells to three main metabolites, two of which had similar retention times to [^{68}Ga]Ga-DFO and [^{68}Ga]Ga-DFO-succinate, respectively. Almost no radioactivity was found in AFU *Δsit1* strain, which lacks the necessary transporter, as shown in Fig. S7 in the supplementary material, proving that the metabolic analysis indeed reflected the fate of the ^{68}Ga-labelled conjugates after active uptake by the siderophore transporter Sit1.

2.4. Uptake assays in AFU cultures

Fig. 4 summarizes the results of the short-term uptake assays after 60 min of incubation time. Both ^{68}Ga-radiolabelled conjugates showed significantly higher accumulation in wild type AFU cultures in iron deplete conditions as compared to controls. Controls were comprised of iron replete media conditions (shaded columns), addition of excess [Fe] ferrioxamine ("block") competing with uptake of ^{68}Ga-labelled conjugates or cultures lacking the siderophore transporter Sit1 ("*Δsit1*"). In cultures with xylose-induced expression of *sit1* ("*sit1*^{xylP}") using an AFU mutant strain described previously [18], uptake was largely independent of iron availability and even higher than in iron deplete wild type cultures. All this indicates specific recognition and uptake of both ^{68}Ga-labelled conjugates **1a** and **2a** by Sit1 as can be expected for derivatives of DFO. Overall, uptake was significantly lower for [^{68}Ga]Ga-conjugate **2a** when compared to[^{68}Ga]Ga-conjugate **1a**, except for wild type cultures under blocking conditions. Uptake in wild type cells under iron-depleted conditions was also significantly lower when compared to [^{68}Ga]Ga-DFO, indicating some impairment of uptake. No statistically significant difference in uptake between [^{68}Ga]Ga-conjugate **1a** and [^{68}Ga]Ga-DFO for wild type iron-depleted cultures could be observed.

2.5. Antifungal activity

Fig. 5 shows the results of MIC assays of the ^{nat}Ga-conjugates **1a** and **2a** in comparison with the inhibitory activity of [^{nat}Ga]Ga-DFO and carboplatin under iron-deplete conditions. 48 h incubation did not reveal any differences. ^{nat}Ga-compounds were used to adhere to local radioprotection guidelines, as this assay does not require radioactive isotopes. Carboplatin did not show any antifungal effect in the applied concentrations, whereas both conjugates inhibited fungal growth

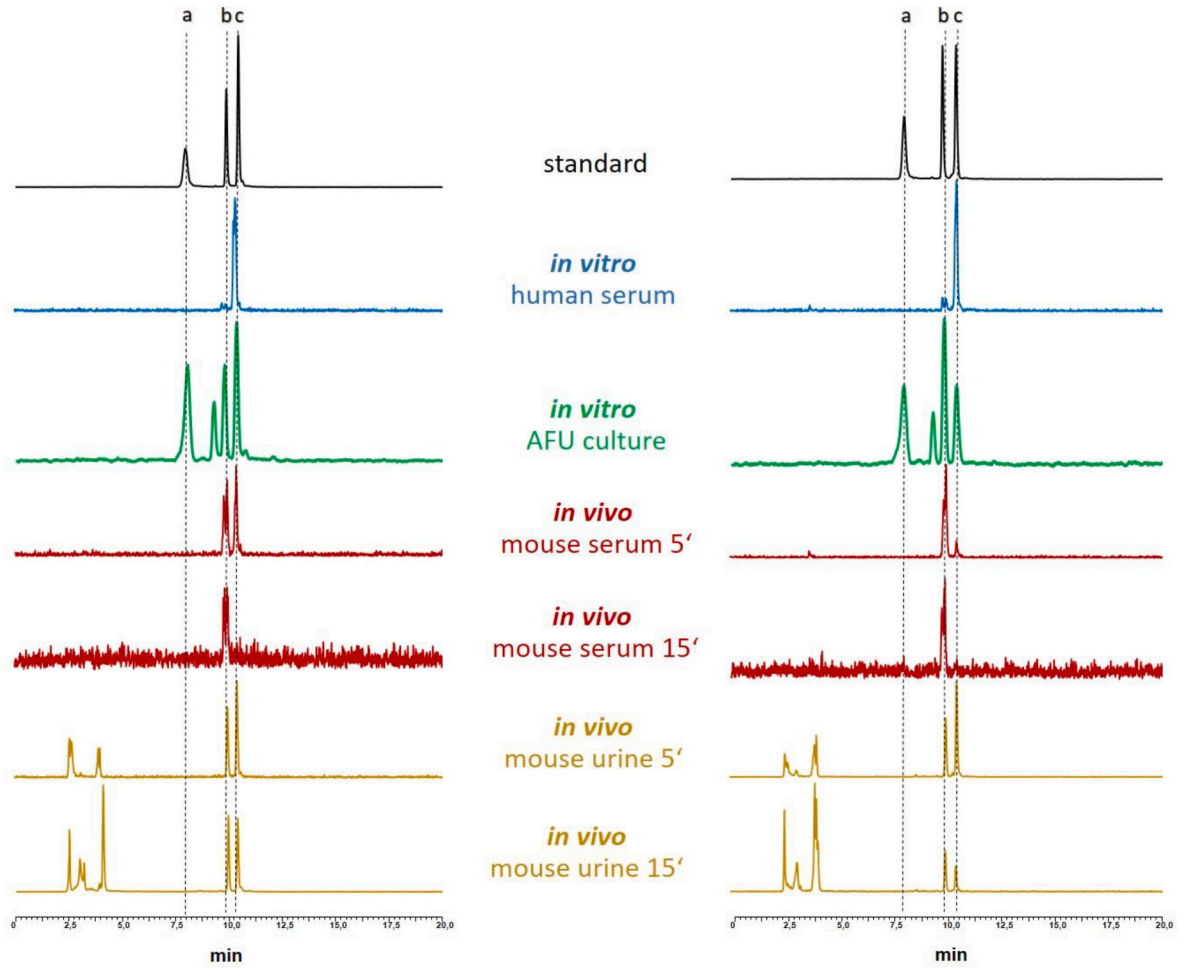

Fig. 3. Stability testing under different conditions: radiochromatograms of ^{68}Ga-labelled conjugates **1a** (left side) and **2a** (right side) *in vitro* in human serum after 60 min incubation (in blue), *in vitro* in AFU cultures after 60 min of incubation (in green) and in serum (red) and urine (yellow) of female BALB/c mice 5 min and 15 min after injection, in comparison with a mixture of [^{68}Ga]Ga-DFO, [^{68}Ga]Ga-DFO-succinate and either [^{68}Ga]Ga-conjugate **1a** or **2a** in solution ("standard"). Letters and dotted lines mark the main metabolites [^{68}Ga]Ga-DFO (a) and [^{68}Ga]Ga-DFO-succinate (b) as well as intact compounds (c).

between 3 and 12 μg/mL concentrations with higher activity of complex **2a**. In comparison, [^{nat}Ga]Ga-DFO showed weaker antifungal activity starting at concentrations higher than 25 μg/mL. MIC assays comparing the antifungal activity in the *sit1*^{xylP} strain (displayed in Fig. S6 in the supplementary material) showed the same pattern of antifungal activities. Even though conjugate **2a** seemed to be slightly more effective under xylose promotion, no significant difference in growth inhibition with or without *sit1* expression could be derived from this control experiment, indicating that the antifungal effect of the conjugates is not primarily dominated by Sit1-mediated uptake. MIC assays under iron-replete conditions showed no growth inhibition for any of the compounds tested.

2.6. Ex vivo biodistribution in mice

The *ex vivo* biodistribution data obtained from mice displayed rapid excretion of both ^{68}Ga-labelled conjugates **1a** and **2a** mainly via the renal system (4.1 ± 0.01 %ID/g for [^{68}Ga]Ga- conjugate **1a** and 4.7 ± 0.97 %ID/g for [^{68}Ga]Ga-conjugate **2a** 30 min p.i. versus 1.2 ± 0.17 % ID/g for [^{68}Ga]Ga-conjugate **1a** and 1.2 ± 0.19 %ID/g for [^{68}Ga]Ga-conjugate **2a** 90 min p.i.) with minimal retention in blood and other organs, even at a short time (30 min) after injection (Table 1). The highest activity concentration in the organs at late time points (90 min p.i.) was found for intestines (1.4 ± 0.46 %ID/g for [^{68}Ga]Ga-conjugate **1a** and 1.3 ± 0.02 %ID/g for [^{68}Ga]Ga-conjugate **2a**), indicative for minor intestinal excretion. The *ex vivo* biodistribution data were fully consistent with the results from animal imaging.

2.7. PET imaging of rat aspergillosis model

Dynamic PET/CT imaging of a rat with pulmonary infection with AFU after injection with ^{68}Ga-labelled conjugates **1a** and **2a** is shown in the supplementary material in Fig. S8. For both compounds, rapid renal elimination was observed with no visible retention in other organs apart from the kidneys. Only the areas of infected lung tissue revealed rapid and increasing uptake of the conjugates over time. This was confirmed by static PET/CT (Fig. 6A) and PET/MR imaging (Fig. 7) with again intense accumulation in infected areas of the rat lung in the PET scan due to accumulation of the [^{68}Ga]Ga-conjugates **1a** and **2a**. The SUV_{max} values for individual animals were 2.87, 1.77 and 1.55 for [^{68}Ga]Ga-conjugate **1a** and 2.40, 2.16 and 1.42 for [^{68}Ga]Ga-conjugate **2a**. Quantitative comparison of lung uptake by means of maximum standardized uptake values (SUV_{max}) showed no significant difference between the two compounds ($p > 0.05$) as shown in Fig. 6B.

3. Discussion

In this study we aimed to repurpose previously developed anticancer Pt(IV)-DFO conjugates for infection targeting therapy. Initial results of our study were very promising. Both Pt(IV)-DFO complexes

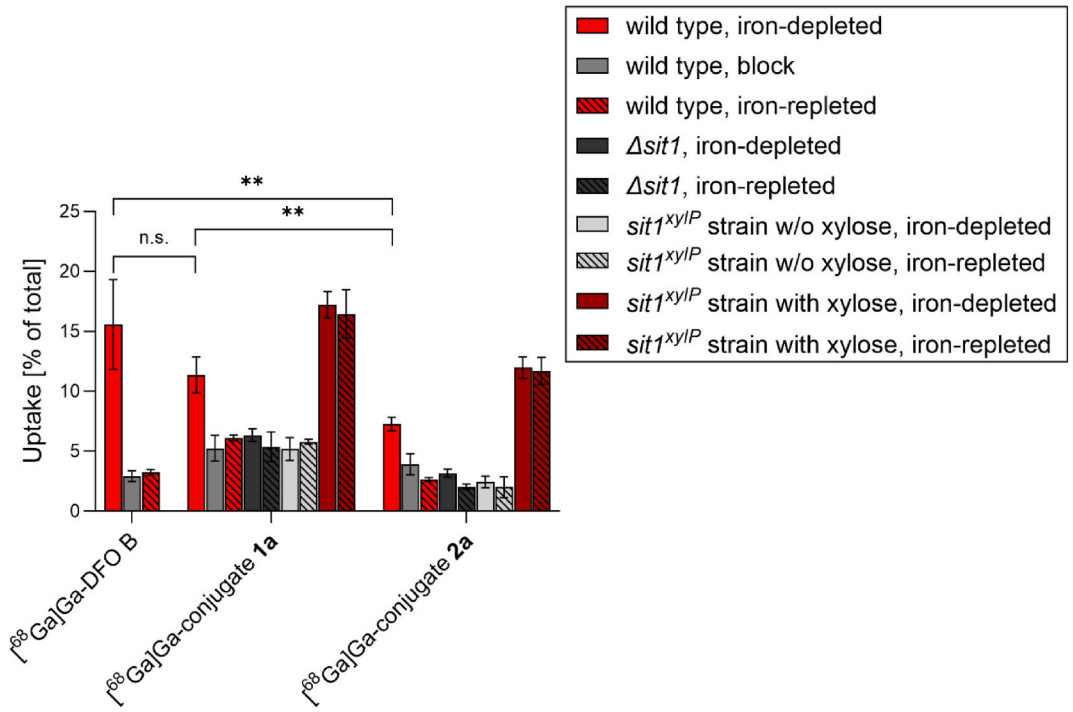

Fig. 4. Short-term uptake assay of ^{68}Ga-labelled Pt(IV)-DFO conjugates in AFU under various conditions. For all compounds an incubation time of 60 min with the denoted cultures was used. Results are given as percent of uptake compared to the total amount of radioactivity added to cultures. AFU strains used were AfS77 ("wild type"), AFU *Δsit1* lacking the gene encoding the Sit1 transporter responsible for DFO uptake, and AFU *sit1*^{xylP} expressing *sit1* under control of the *xylP* promoter (*PxylP*) allowing repression in the absence and induction in the presence of 1 % xylose in the growth medium, largely independent of iron availability (n = 4 for all conditions). Stastitical significance between values for wild type iron-depleted conditions are denoted as: n.s. = non-significant ($p > 0.05$), ** = $p < 0.01$.

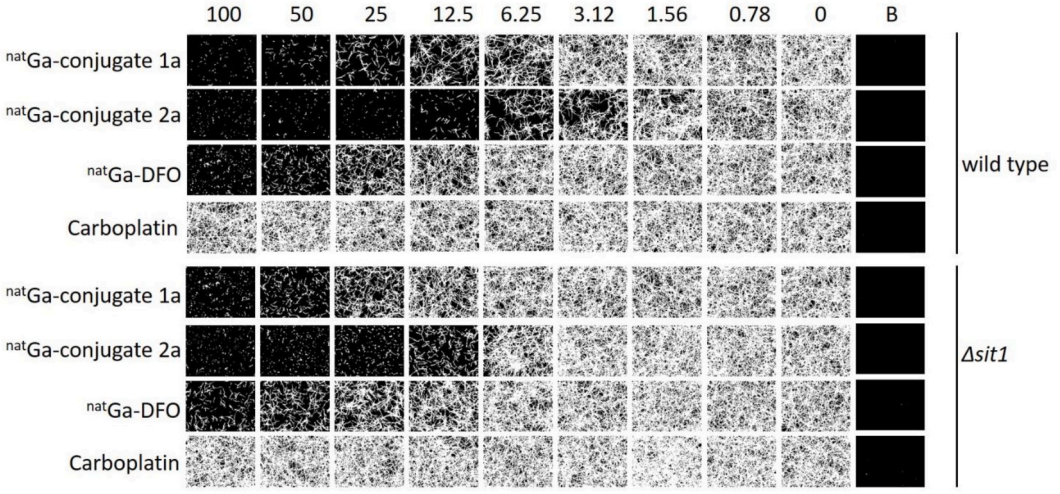

Fig. 5. MIC assay results for ^{nat}Ga-conjugates **1a** and **2a** in AFU wild type and *Δsit1* strain at 24 h incubation time under iron-deplete conditions. Numbers in the top row denote concentrations of compounds in μg/mL. [^{nat}Ga]Ga-DFO and carboplatin were used as controls for antifungal activity. B = blank (no AFU spores added).

could be labelled quantitatively with gallium-68, showing only a radiochemical impurity that corresponded to [^{68}Ga]Ga-DFO-succinate. The proportion of this impurity was higher for Pt(IV)-DFO conjugate **2a** compared to **1a**, suggesting slightly reduced stability when hemi-succinate is used as the second axial ligand instead of acetate. After radiolabelling no degradation of the main peak in solution or in human serum was observed, indicating a high stability. Protein binding studies also showed very low levels of bound fractions with values < 10 %. This stability reflected the *in vivo* pharmacokinetic behaviour with predominant and rapid renal excretion without retention or accumulation in any organ except the kidneys, overall very similar to the pharmacokinetics of [^{68}Ga]Ga-DFO itself and with no difference between the two conjugates under investigation. The accumulation in pulmonary infection areas was also rapid and allowed a clear delineation of the infected tissue minutes after injection, which could be shown by PET imaging, indicating specific uptake by SITs overexpressed by the invading pathogen. This reflected the *in vitro* results in AFU cultures where significantly higher uptake was observed in cultures with *sit1* expression as compared to several controls, where *sit1* was either not expressed due to iron sufficient conditions, blocked by excess of ferrioxamine or deleted. The slightly higher *in vitro* uptake of ^{68}Ga-labelled conjugate **1a**, which could be expected due to its second axial ligand (acetate) that cannot be

Table 1
Data sets of *ex vivo* biodistribution studies performed in mice. Results for ^{68}Ga-labelled conjugates **1a** and **2a** are given as percentage of injected dose per gram (%ID/g) for 30 min and 90 min time points after injection. Values are given as means ± standard deviation of three animals per compound and time point (n = 3).

	[^{68}Ga]Ga-conjugate 1a		[^{68}Ga]Ga-conjugate 2a	
	30 min	90 min	30 min	90 min
blood	1.22 ± 0.03	0.20 ± 0.01	1.52 ± 0.25	0.23 ± 0.02
spleen	0.34 ± 0.04	0.08 ± 0.01	0.45 ± 0.08	0.11 ± 0.01
pancreas	0.33 ± 0.03	0.06 ± 0.00	0.44 ± 0.04	0.05 ± 0.01
stomach	0.62 ± 0.02	0.17 ± 0.04	0.85 ± 0.15	0.14 ± 0.04
intestine	1.16 ± 0.12	1.44 ± 0.46	1.49 ± 0.04	1.32 ± 0.02
kidneys	4.09 ± 0.01	1.23 ± 0.18	4.71 ± 0.97	1.20 ± 0.19
liver	0.98 ± 0.07	0.30 ± 0.09	1.10 ± 0.19	0.24 ± 0.04
heart	0.47 ± 0.03	0.10 ± 0.01	0.60 ± 0.06	0.10 ± 0.00
lung	1.25 ± 0.07	0.23 ± 0.02	1.55 ± 0.14	0.25 ± 0.01
muscle	0.22 ± 0.02	0.05 ± 0.02	0.25 ± 0.04	0.04 ± 0.01
femur	0.23 ± 0.08	0.11 ± 0.02	0.30 ± 0.02	0.07 ± 0.00

deprotonated at pH 7.4, unlike the hemisuccinate axial ligand in compound **2a**, was however not observed *in vivo*. Instead, quantitative uptake values in the infected areas were not significantly different.

When looking at the antifungal activities of the compounds, the lowest MIC values at about 3 μg/mL were found for conjugate **2a**, which indicated a higher antifungal activity than any of the TAFC conjugates studied previously [14,19] and compares to MIC values of 0.5–1 μg/mL for the standard antifungals itraconazole or voriconazole [10]. Conjugate **1a** was only slightly less active, with both compounds showing significantly more growth inhibition than [^{nat}Ga]Ga-DFO itself. This observed difference correlates to a slightly lower *in vivo* stability of **2a,** indicative for facilitated release of platinum with subsequent formation of carboplatin. All these studies used the respective gallium complexes, as the free ligands should not be recognized by SITs and iron complexes can have an overlapping growth promotion effect due to the delivery of essential iron. Carboplatin itself did not show any antifungal activity in this setting, indicating a Sit1-dependent antifungal activity of the compounds under study. However, using the *sit1*^{xylP} strain allowed a more in-depth investigation of the mechanism of antifungal activity. In this strain *sit1* is only expressed when xylose is added to the culture. In this setting only a minor, non-significant difference between *sit1* expressing and *sit1* suppressing conditions in relation to the antifungal effect of the conjugates was found, even though uptake was significantly higher, as shown with the Ga-68 versions in the short term uptake assays. This indicates, together with the observation of antifungal activity of [^{nat}Ga]Ga-DFO itself, a predominant effect of the Ga-complexation independent of *sit1* expression. Similar effects of gallium were also observed in our recent study with other conjugates. Nevertheless, the relatively high overall antifungal effect is promising and so far, was not reached in our attempt to develop SIT-specific antifungal agents.

We also conducted an in-depth investigation into the processing of the compounds under study. While both radiolabelled conjugates **1a** and **2a** were stable in human serum and mouse tissue homogenates *in vitro*, they underwent rapid metabolism *in vivo*, resulting in non-detectable levels of intact compound in serum already 15 min after injection as well as a high levels of metabolites in urine. In comparison, [^{68}Ga]Ga-conjugate **2a** showed overall lower stability in our *in vivo* experiments than [^{68}Ga]Ga-conjugate **1a**. Rapid renal elimination and accumulation in blood cells may have also contributed to the fast decline in serum levels of the parent compounds. Studies on the clinically tested Pt(IV) complex satraplatin in whole human blood have indicated rapid biotransformation upon reduction by red blood cells metal-containing redox proteins [20,21], whereas hydrophilic carboplatin-based Pt(IV) complexes have shown no signs of extracellular reductive biotransformation in whole blood (in *in vitro* experiments) [22]. At this stage, it is unclear whether the *in vivo* release of ^{68}Ga-labelled DFO-succinate is due to hydrolysis or reduction of complexes **1a** and **2a,** and whether it occurs mainly in the liver or in the blood cells. The same metabolite was also found in urine together with other ^{68}Ga-labelled species eluting earlier

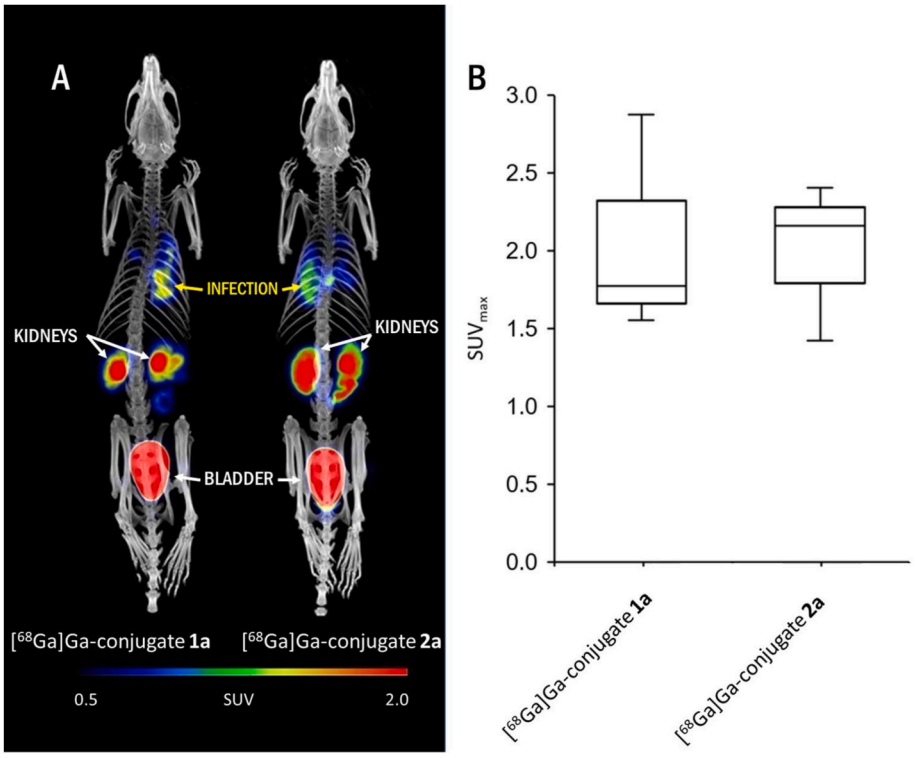

Fig. 6. (A) Static PET/CT imaging of rats with AFU lung infection, performed 45 min after injection of [^{68}Ga]Ga-conjugate **1a** and [^{68}Ga]Ga-conjugate **2a**, showing rapid accumulation in infected lung tissue alongside pronounced renal uptake related to elimination of the compounds. (B) Comparison of radioactive signal uptake in the lungs of AFU-infected rats (n = 3). Results are expressed as SUV_{max}.

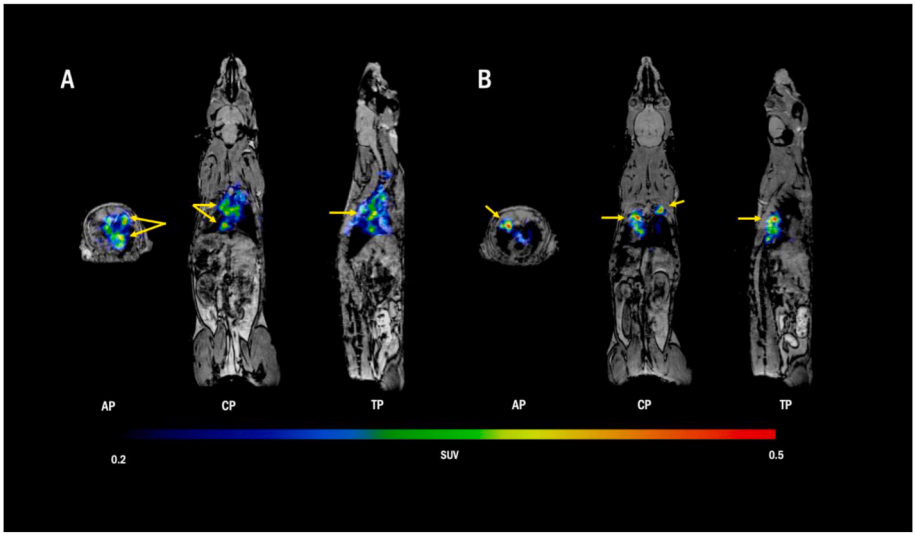

Fig. 7. Static PET/MRI imaging of rats with AFU lung infection, injected with (A) [^{68}Ga]Ga-conjugate **1a** and (B) [^{68}Ga]Ga-conjugate **2a** 60 min p.i. Whole body MRI images fused with PET images of lung area only, showing clear accumulation in infected lung tissues (yellow arrows). AP = axial projection; CP = coronal projection; TP = transversal projection.

on RP-HPLC.

However, we could clearly identify significant degradation of both ^{68}Ga-labelled conjugates **1a** and **2a** in fungal cells expressing *sit1 in vitro*, with two major metabolites having the same retention time as ^{68}Ga-labelled DFO and ^{68}Ga-labelled DFO-succinate, but still intact conjugates being present. This finding indicates delivery of the intact platinum(IV)-DFO complexes into the fungal cell and intracellular metabolism with potential release of carboplatin. Together with the lack of uptake in cultures lacking Sit1 *in vitro* this supports the concept of fungal-specific delivery and activation of the drug.

The use of DFO as a targeting moiety in Pt(IV) complexes holds the advantage of specifically targeting life threatening fungal infections, but can also be used in case of bacterial infections, where a number of both gram-positive and gram-negative pathogenic bacteria are known to express SITs recognizing DFO. However, this study also revealed some of the limitations of this approach. First, stability of the compounds has to be carefully studied, particularly considering the *in vivo* situation, were a delicate balance of high stability for targeted delivery and efficient release of the antimicrobial vector at the target has to be found. Second, antimicrobial activity should also be investigated in relation to the proposed mechanism in particular when a targeted delivery is envisaged. Our study shows that further research into optimising multifunctional platinum(IV) complexes for antimicrobial use is required.

4. Conclusion

In this paper we could show that multifunctional platinum(IV)-DFO complexes, designed for anticancer treatment, can be reutilized for targeted microbial imaging and treatment in a combined theranostic approach. This concept takes advantage of specific transport via Sit1 using DFO as a targeting moiety. Our results showed fast radiolabelling with gallium-68 under mild conditions with high radiochemical purity, low protein binding properties and high stability in human serum. The compounds showed uptake equal to or slightly less than ^{68}Ga-radiolabelled DFO in AFU wild type cells, with significantly lower uptake in AFU mutants lacking *sit1*. Moderate antifungal activity, not solely dependent on Sit1-expression, as determined by MIC assays was observed. *In vivo* assays in healthy mice and small animal PET imaging using a rat pulmonary aspergillosis model indicated favourable pharmacokinetics with rapid biodistribution and accumulation in infected tissue as well as renal excretion. However, the apparent fast metabolism of the investigated compounds and the observation that antimicrobial activity was not exclusively Sit1-dependent require further optimisation of this approach. Nevertheless, it shows great promise, particularly with regard to the favourable pharmacokinetics and the overall good antifungal properties of the compounds studied, which opens up the possibility of developing targeted antimicrobial theranostic agents.

5. Experimental section

5.1. Chemicals and reagents

All chemicals were purchased from Merk-Sigma Aldrich as reagent grade and used without further purification unless stated otherwise.

Platinum(IV)-DFO conjugates **1** and **2** were synthesized as previously described [2]. DFO-Succinate was prepared by reacting deferoxamine mesylate with succinic anhydride and N,N-diisopropylethylamine (DIPEA) in anhydrous DMF, following literature procedures [23] with minor adjustments. The reaction afforded the desired product in 85 % yield. The identity and purity (>95 %) of the compounds were confirmed by ^{1}H NMR, ESI-HRMS and RP-HPLC. Stable gallium (^{nat}Ga)-containing platinum(IV)-DFO conjugate complexes as well as [^{nat}Ga]Ga-DFO as a reference substance for MIC assays were produced by reacting a 5-fold molar excess of $^{nat}GaBr_3$ in acetate buffer pH 4.5 with 1 mg of the respective platinum(IV)-DFO conjugate or DFO alone for 10 min at room temperature, followed by removal of unbound gallium using a C-18 cartridge (SEP-PAK light, Waters Cooperation, Milford, MA). The resulting ^{nat}Ga-complexes were analysed by HPLC and MS.

5.2. Radiolabelling and analysis

Gallium-68 was produced by fractionated elution of ^{68}Ge/^{68}Ga-generator (IGG100. Eckert & Ziegler Isotope Products, Berlin, Germany; nominal activity of 1850 MBq) with 0.1 M hydrochloric acid (HCl, Rotem Industries, Arva, Israel). For labelling, 10 μg (8.6–9.0 nmol) of platinum(IV)-DFO conjugates **1** and **2** were mixed with 200 μL gallium-68 eluate (~15–30 MBq) and the pH was adjusted to 4.5 by adding 20 μL of sodium acetate solution (1.14 M) per 100 μL eluate. The mixture was left to react for 10 min at room temperature and afterwards analysed by radio-TLC and radio-RP-HPLC [8,9]. Radiolabelling of DFO and DFO-succinate with gallium-68 as reference substances for assays was performed likewise.

RP-HPLC analysis was performed with the following

instrumentation: UltiMate 3000 RS UHPLC pump, UltiMate 3000 autosampler, Ultimate 3000 column compartment (25 °C oven temperature), UltiMate 3000 variable wavelength detector (Thermo Fisher, Germering, Germany; UV detection at λ = 220 nm), GABI Star radiometric detector (Raytest GmbH, Straubenhardt, Germany), NUCLEODUR 100-5 C18 ec, 5 μm, 250 × 4.6 mm (Macherey - Nagel, Dueren, Germany) column with acetonitrile (ACN)/H_2O/0.1 % trifluoroacetic acid (TFA) as mobile phase; flow rate of 1 mL/min; gradient 0.0−3.0 min 10 % ACN, 3.0−16 min 10−60 % ACN, 16.0−18.0 min 60 % ACN and re-equilibration of the column with 10 % ACN afterwards. Radiolabelling efficiency and RCP were additionally analysed by ITLC-SG (Varian, Lake Forest, CA, USA) with either a 0.1 M citrate buffer pH 5 as mobile phase or a mixture of methanol and ammonium acetate 1 M (1:1 $^{v}/_{v}$) as mobile phase. ITLC-SG strips were scanned using a Radio-TLC-Scanner (Scan-RAM, Lablogic, Sheffield, UK). ESI-MS experiments were carried out with LCMS-2050 Nexera (Shimadzu, Kyoto, Japan) using the following conditions: scan range (*m/z* 400.0–2000; sampling 500 msec/2 Hz; mobile phase: 30 % water and 70 % acetonitrile with 0.1 % formic acid; flow rate: 0.5 mL/min). Data were acquired and evaluated with LabSolutions software (Shimadzu, Kyoto, Japan).

5.3. In vitro characterization

5.3.1. Protein binding

For this procedure platinum(IV)-DFO conjugates were labelled with Ga-68 as described before and diluted with PBS to a concentration of approximately 9 μM. Fresh human serum was obtained from routine blood withdrawal procedures of one of the co-authors, giving informed consent for the use in the described experiments. 5 mL of blood were collected in serum tubes (Serum CAT S-Monovette, Sarstedt, Germany) and were centrifuged 15 min after withdrawal. The serum was collected in the supernatant. 50 μL of the solution containing ^{68}Ga-labelled platinum(IV)-DFO conjugates were added to 450 μL of PBS (control) or 450 μL of fresh human serum (n = 2) and incubated at 37 °C for 15, 30 and 60 min. At each timepoint 25 μL of PBS/serum was analysed by size exclusion chromatography using MicroSpin G-50 columns (Sephadex G-50, GE Healthcare, Vienna, Austria) according to the manufacturer's protocol. Hereafter, the column and eluate were measured separately in a gamma counter (2480 Wizard2 3″, PerkinElmer Life Sciences and Analytical Sciences, formerly Wallac Oy, Turku, Finland) and percentage of protein bound conjugate were calculated by dividing measured radioactivity in the eluate as counts per minute (cpm) by the total activity added according to this formula: **cpm eluate/(cpm column + cpm eluate)*100**. Radioactivity in the eluates reflect protein bound fraction and column bound, radiolabelled conjugate **1a** or **2a**. Experiments were performed in duplicates (n = 2).

5.3.2. Serum and enzymatic stability

Serum stability probes were prepared according to the protein binding section with PBS and fresh human serum. After 15, 30 and 60 min, 100 μL of serum/PBS were mixed with 100 μL of methanol to precipitate proteins in the serum. Hereafter, the mixture was centrifuged for 1 min and 100 μL of the supernatant were diluted with water and analysed by radio-HPLC to determine intact labelled platinum(IV)-DFO conjugates. To assess enzymatic stability in kidney and liver homogenates, kidneys or liver freshly excised from BALB/c mice were rapidly rinsed and homogenised in 20 mM HEPES buffer pH 7.3 with an Ultra-Turrax T25 disperser (IKA-Werke GmbH, Staufen, Germany) for 1 min at RT. The radioconjugates were incubated with fresh 30 % homogenates at 37 °C for up to 2 h. Samples were precipitated with methanol, centrifuged (1750 *g*, 5 min), and analysed by HPLC using the same chromatographic conditions as stated in section "radiolabelling and analysis".

5.3.3. Uptake and competition assay

The following AFU strains as described in Refs. [15,18] were used: AFU AfS77, termed wild type here, AFU *Δsit1*, which lacks the gene encoding the Sit1 transporter responsible for DFO uptake, and AFU *sit1^{xylP}*, which expresses *sit1* under control of the *xylP* promoter (*PxylP*) allowing repression in the absence and induction in the presence of 1 % xylose in the growth medium, largely independent of iron availability [24].

Short-term uptake assays were performed as previously published [6]. Briefly, 180 μL of the respective AFU culture in iron-depleted and iron-repleted (control – transporter suppression) Aspergillus minimal media (AMM) [25] as well as after addition of 10 μM [Fe]ferrioxamine to the iron deplete culture (Sit1-blocking condition) were added in pre-wetted 96-well MultiScreen Filter Plates HTS (1 μm glass fiber filter, Merck Millipore, Darmstadt, Germany) and incubated for 15 min at 37 °C with either 25 μL PBS or 25 μL [Fe]DFO solution (control – uptake block; ~10 μM). Hereafter, 50 μL of radiolabelled compound (final concentration approximately 90 nM) was added and incubated for another 45 min at 37 °C. Four probes for each compound and condition were prepared (n = 4). Hyphae were washed two times with ice cold TRIS buffer and dry filters were measured in a gamma counter. Uptake by cells was calculated as percentage of counts in relation to 50 μL standards of radiolabelled compounds, which were directly measured in the gamma counter.

5.3.4. Stability in AFU cultures

As described for the uptake and competition assays, AFU wild type and AFU *Δsit1* strains were used. ^{68}Ga-labelled conjugates **1a** and **2a** were incubated for 60 min with 2 mL of the respective AFU cultures in iron-depleted Aspergillus minimal media (AMM) and sodium acetate solution (1.1 M) for pH adjustment of the mixture to around 4.5. Afterwards, cultures were filtered and washed with PBS three times. The cultures were then resuspended in 1 mL of PBS and homogenised with an Ultra-Turrax T25 disperser (IKA-Werke GmbH, Staufen, Germany) for 2 min at RT. 1 mL of methanol was added to each sample to precipitate proteins and other cell components. Samples were then centrifuged for 3 min and the supernatants diluted 1:1 with water before HPLC analysis.

5.3.5. Minimal inhibitory concentration assay (MIC)

MIC assays were performed in analogy to CLSI guidelines with minor modifications [26]. In brief, 96-well plates (Greiner Bio-One GmbH, Kremsmünster, Austria) were prepared with 100 μL of either iron-depleted [Fe(−)] or iron-repleted [Fe(+)] 2 x AMM containing $3*10^4$ spores per well of AFU strains as described above in the uptake and competition assays section. 100 μL of either the ^{nat}Ga-complex of siderophore conjugates, ^{nat}Ga-DFO or carboplatin, was added to get a final concentration of 1 x AMM medium and antifungal ranging from 0.78 to 100 μg/mL. The lowest concentration without visible growth was used to determine the MIC value after incubation for 24 h and 48 h at 37 °C in a humidity chamber [19]. Results were also displayed by preforming microscopy pictures of each well after 24 h. Images were acquired with the IncuCyte S3 Live-Cell Analysis System equipped with a 20x magnification S3/SX1 G/R Optical Module (Essen BioScience Inc.). From each well a representative image was taken from the center of the well. Fungal growth was analysed using the Basic Analyzer tool (Confluence %; Segmentation adjustment: 0; Adjust Size: 0) of the IncuCyte S3 software (Version 2019; Essen BioScience Inc., Ann Arbor, Michigan, USA). Images and confluence mask were exported in raw 8-bit images and raw 8-bit confluence mask, respectively.

5.4. In vivo characterization

All animal experiments were conducted in compliance with the Austrian and Czech animal protection laws and with approval of the Austrian Ministry of Science (BMWFW-66.011/0161-WF/V/3b/2016), the Czech Ministry of Education Youth and Sports (MSMT-24421/2021-4) and the institutional Animal Welfare Committee of the Faculty of Medicine and Dentistry of Palacký University in Olomouc.

5.4.1. *In vivo stability and ex vivo biodistribution*

Stability test and biodistribution were conducted in 8–10 weeks old female BALB/c mice (Charles River Laboratories, Sulzfeld, Germany). ^{68}Ga-labelled conjugates **1a** and **2a** were injected via the lateral tail vein using approximately 0.4 nmol of siderophore conjugate for the evaluation of their *in vivo* stability.

In vivo stability was determined by radio-HPLC analysis. After injection of the radiolabelled compound (~12 MBq) the mouse was euthanized after 5 and 15 min by cervical dislocation. Blood was collected and precipitated with methanol to remove blood cells and proteins. Subsequently, the supernatant was diluted with water and used for further analysis. Urine samples were centrifuged and directly injected into the radio-HPLC. Percentage of intact radiolabelled siderophore conjugate was calculated by integration of the radio-chromatogram [27]. For the *ex vivo* biodistribution study, mice were injected retro-orbitally (r.o.) with ^{68}Ga-labelled conjugates **1a** or **2a** (~2 MBq/mouse, approximately ~1 μg of conjugate). Mice were sacrificed by cervical dislocation 30 min and 90 min post-injection (p.i.). Organs and tissues of interest (blood, spleen, pancreas, stomach, intestine, kidneys, liver, heart, lung, muscle and femur) were removed and weighed. The amount of radioactivity in the samples was measured in the gamma counter. Results were expressed as percentage of injected dose per gram of organ (%ID/g).

5.4.2. *Invasive pulmonary aspergillosis model in rats*

2–3 months old female Lewis rats were treated with the immunosuppressant cyclophosphamide (Endoxan, Baxter, 75 mg/kg i.p.) 5 days and 1 day before being infected with AFU, to induce neutropenia. The animals repeatedly (5 days, 1 day before and on the day of inoculation) received the antibiotic teicoplanin (Targocid, Sanofi, 35 mg/kg–5 days before i.m. or 25 mg/kg i.m.–1 day before and on the day of inoculation) to avoid bacterial superinfections and additional antibiotics were administered by drinking water (Ciprofloxacin, 2 mM, Polymyxin E, Colomycin, 0.1 mM) for the duration of the experiment. Infection in the lung was established by intratracheal inoculation of 100 μL of AFU spores (10^9 CFU/mL AFU 1059 CCF) using TELE PACK VET X LED system equipped with a rigid endoscope (Karl Stroz GmbH & Co. KG, Tuttlingen, Germany) only [28].

5.4.3. *Imaging studies*

Anesthetized AFU infected rats were r.o. injected with ^{68}Ga-labelled conjugates **1a** or **2a** (~10 MBq/rat, approximately ~2.5 μg of conjugate) and placed in the prone position in the respective imaging systems. Dynamic μPET/CT imaging was performed on a Mediso NanoScan PET/CT imaging system for small animals (Mediso Medical Imaging Systems, Budapest, Hungary). Double FOV (2 × 98.55 mm) PET scan was acquired immediately after injection to 60 min p.i., followed by whole-body helical CT (50 kVp/908 μA, 720 projections). Static μPET/3T MRI imaging was performed for approximately 30 min with double FOV PET scan (2 × 98.5 mm), followed by a coronal T1-weighted 3D gradient echo scan (slice thickness = 0.6 mm; TR = 15 ms; TE = 3.9 ms; NEX = 2; flip angle = 20°) 60 min p.i. using the Mediso NanoScan PET/MRI 3T small animal imaging system (Mediso Medical Imaging Systems, Budapest, Hungary). Static μPET/CT imaging was performed for approximately 25 min with double FOV PET scan (2 × 98.5 mm), followed by whole-body helical CT (50 kVp/908 μA, 720 projections) at 45 min p.i. using the Mediso NanoScan PET/CT system mentioned above. Image reconstruction for data from both scanners was performed using Mediso Tera-Tomo iterative 3D PET reconstruction (Mediso Medical Imaging Systems, Budapest, Hungary). Image visualization, processing, and quantification were performed with Mediso InterView FUSION software (Mediso Medical Imaging Systems, Budapest, Hungary). All images were normalized to the injected activity and animal weight.

CRediT authorship contribution statement

Martin Kraihammer: Writing – original draft, Visualization, Investigation, Formal analysis. **Hristo P. Varbanov:** Writing – review & editing, Validation, Resources, Formal analysis, Conceptualization. **Kateřina Dvořáková Bendová:** Writing – review & editing, Validation, Investigation, Formal analysis. **Miloš Petřík:** Writing – review & editing, Validation, Supervision, Resources, Methodology, Funding acquisition, Formal analysis. **Annie Yap:** Writing – review & editing, Investigation, Formal analysis. **Giacomo Gariglio:** Visualization, Data curation. **Hubertus Haas:** Writing – review & editing, Supervision, Resources, Formal analysis, Conceptualization. **Clemens Decristoforo:** Writing – review & editing, Writing – original draft, Validation, Supervision, Methodology, Investigation, Conceptualization.

Funding

We gratefully acknowledge the financial support of the project National Institute of Virology and Bacteriology (Programme EXCELES, ID Project No. LX22NPO5103)—Funded by the European Union—Next Generation EU, the Czech Ministry of Education, Youth and Sports through projects EATRIS ((LM2023053) and Czech-BioImaging (LM2023050), and the Czech Science Foundation, grant number 24–14579L.

Declaration of competing interest

The authors declare the following financial interests/personal relationships which may be considered as potential competing interests: Milos Petrik reports financial support was provided by European Union. Milos Petrik reports financial support was provided by European Infrastructure for Translational Medicine. Milos Petrik reports financial support was provided by Czech Science Foundation. If there are other authors, they declare that they have no known competing financial interests or personal relationships that could have appeared to influence the work reported in this paper.

Acknowledgements

We want to thank the staff of the Animal Facilities of the Institute of Molecular and Translational Medicine of Faculty of Medicine and Dentistry of Palacký University in Olomouc for their care of animals. We also acknowledge Sophia Harringer for the synthesis of complex **1**.

Appendix A. Supplementary data

Supplementary data to this article can be found online at https://doi.org/10.1016/j.ejmech.2025.118216.

Data availability

Data will be made available on request.

References

[1] H.P. Varbanov, F. Kuttler, D. Banfi, G. Turcatti, P.J. Dyson, Repositioning approved drugs for the treatment of problematic cancers using a screening approach, PLoS One 12 (2017) e0171052, https://doi.org/10.1371/journal.pone.0171052.
[2] S. Harringer, M. Hejl, É.A. Enyedy, M.A. Jakupec, M.S. Galanski, B.K. Keppler, et al., Multifunctional Pt(iv) prodrug candidates featuring the carboplatin core and deferoxamine, Dalton Trans. 50 (2021) 8167–8178, https://doi.org/10.1039/d1dt00214g.
[3] C. Imberti, J. Lok, J.P.C. Coverdale, O.W.L. Carter, M.E. Fry, M.L. Postings, et al., Radiometal-labeled photoactivatable Pt(IV) anticancer complex for theranostic phototherapy, Inorg. Chem. 62 (2023) 20745–20753, https://doi.org/10.1021/acs.inorgchem.3c02245.
[4] M. Petrik, E. Umlaufova, V. Raclavsky, A. Palyzova, V. Havlicek, J. Pfister, et al., 68Ga-labelled desferrioxamine-B for bacterial infection imaging, Eur. J. Nucl. Med. Mol. Imag. 48 (2021) 372–382, https://doi.org/10.1007/s00259-020-04948-y.

[5] Q. Laurent, L.K. Batchelor, P.J. Dyson, Applying a trojan horse strategy to ruthenium complexes in the pursuit of novel antibacterial agents, Organometallics 37 (2018) 915–923, https://doi.org/10.1021/acs.organomet.7b00885.
[6] M. Misslinger, M. Petrik, J. Pfister, I. Hubmann, K. Bendova, C. Decristoforo, et al., Desferrioxamine B-mediated pre-clinical in vivo imaging of infection by the mold fungus Aspergillus fumigatus, J Fungi (Basel) 7 (2021) 734, https://doi.org/10.3390/jof7090734.
[7] S. Moura, L. Cerqueira, A. Almeida, Invasive pulmonary aspergillosis: current diagnostic methodologies and a new molecular approach, Eur. J. Clin. Microbiol. Infect. Dis. 37 (2018) 1393–1403, https://doi.org/10.1007/s10096-018-3251-5.
[8] J.D. Jenks, M. Hoenigl, Treatment of aspergillosis, J Fungi (Basel) 4 (2018) 98, https://doi.org/10.3390/jof4030098.
[9] J. Lai, B. Wang, M. Petrik, N. Beziere, D.A. Hammoud, Radiotracer development for fungal-specific imaging: past, present, and future, J. Infect. Dis. 228 (2023) S259–S269, https://doi.org/10.1093/infdis/jiad067.
[10] C.O. Morrissey, H.Y. Kim, T.-M.N. Duong, E. Moran, A. Alastruey-Izquierdo, D. W. Denning, et al., Aspergillus fumigatus-a systematic review to inform the World Health Organization priority list of fungal pathogens, Med. Mycol. 62 (2024) myad129, https://doi.org/10.1093/mmy/myad129.
[11] M. Petrik, J. Pfister, M. Misslinger, C. Decristoforo, H. Haas, Siderophore-based molecular imaging of fungal and bacterial infections-current status and future perspectives, J Fungi (Basel) 6 (2020) 73, https://doi.org/10.3390/jof6020073.
[12] B.Z. Sim, S. Levy, M. Haskali, C. Decristoforo, H. Haas, B. Emmerson, et al., P-2126. 'SPECIFIC' first-in-human clinical trial of 68Ga-triacetylfusarinine (TAFC) siderophore PET/CT for detection of invasive aspergillosis, Open Forum Infect. Dis. 12 (2025) ofae631.2282, https://doi.org/10.1093/ofid/ofae631.2282.
[13] C. Decristoforo, M. Mann, B. Nilica, S. Rauch, G. DiSanto, M. Petrik, et al., Safety, pharmacokinetics, radiation dosimetry and preliminary diagnostic performance of [68Ga]Ga-deferoxamin in patients with bacterial infections - results from a Phase I/IIa study. EANM'24 Abstract Book Congress Oct 19-23, 2024, Eur. J. Nucl. Med. Mol. Imag. 51 (2024) 331, https://doi.org/10.1007/s00259-024-06838-z.
[14] J. Pfister, M. Petrik, K. Bendova, B. Matuszczak, U. Binder, M. Misslinger, et al., Antifungal siderophore conjugates for theranostic applications in invasive pulmonary aspergillosis using low-molecular TAFC Scaffolds, J Fungi (Basel) 7 (2021) 558, https://doi.org/10.3390/jof7070558.
[15] M. Aguiar, T. Orasch, M. Misslinger, A.-M. Dietl, F. Gsaller, H. Haas, The siderophore transporters Sit1 and Sit2 are essential for utilization of Ferrichrome-, ferrioxamine- and coprogen-type siderophores in Aspergillus fumigatus, J Fungi (Basel) 7 (2021) 768, https://doi.org/10.3390/jof7090768.
[16] N.A. Hummell, N.V. Kirienko, Repurposing bioactive compounds for treating multidrug-resistant pathogens, J. Med. Microbiol. 69 (2020) 881–894, https://doi.org/10.1099/jmm.0.001172.
[17] K. Joyce, S. Saxena, A. Williams, C. Damurjian, N. Auricchio, S. Aluotto, et al., Antimicrobial spectrum of the antitumor agent, cisplatin, J. Antibiot. 63 (2010) 530–532, https://doi.org/10.1038/ja.2010.64.
[18] A.-M. Dietl, M. Misslinger, M.M. Aguiar, V. Ivashov, D. Teis, J. Pfister, et al., The siderophore transporter Sit1 determines susceptibility to the antifungal VL-2397, Antimicrob. Agents Chemother. 63 (2019) e00807, https://doi.org/10.1128/AAC.00807-19.
[19] J. Pfister, R. Bata, I. Hubmann, A.A. Hörmann, F. Gsaller, H. Haas, et al., Siderophore scaffold as carrier for antifungal peptides in therapy of Aspergillus fumigatus infections, Journal of Fungi 6 (2020) 367, https://doi.org/10.3390/jof6040367.
[20] J. Carr, M. Tingle, M. McKeage, Rapid biotransformation of satraplatin by human red blood cells in vitro, Cancer Chemother. Pharmacol. 50 (2002) 9–15, https://doi.org/10.1007/s00280-002-0462-2.
[21] J.L. Carr, M.D. Tingle, M.J. McKeage, Satraplatin activation by haemoglobin, cytochrome C and liver microsomes in vitro, Cancer Chemother. Pharmacol. 57 (2006) 483–490, https://doi.org/10.1007/s00280-005-0069-5.
[22] S. Theiner, M. Grabarics, L. Galvez, H.P. Varbanov, N.S. Sommerfeld, M. S. Galanski, et al., The impact of whole human blood on the kinetic inertness of platinum(iv) prodrugs – an HPLC-ICP-MS study, Dalton Trans. 47 (2018) 5252–5258, https://doi.org/10.1039/C7DT04537A.
[23] D.E. Carrera, T. Nguyen, C. Medley, Y. Li, R. Angelaud, F. Gosselin, Process development of the synthesis and purification of a reactive immuno-PET conjugate intermediate, Org. Process Res. Dev. 20 (2016) 312–318, https://doi.org/10.1021/acs.oprd.5b00379.
[24] A. Yap, I. Glarcher, M. Misslinger, H. Haas, Characterization and engineering of the xylose-inducible xylP promoter for use in mold fungal species, Metab Eng Commun 15 (2022) e00214, https://doi.org/10.1016/j.mec.2022.e00214.
[25] G. Pontecorvo, J.A. Roper, L.M. Chemmons, K.D. Macdonald, A.W.J. Bufton, The Genetics of Aspergillus nidulans, Adv. Genet. (1953) 141–238, https://doi.org/10.1016/S0065-2660(08)60408-3.
[26] Clinical and Laboratory Standards Institute, Reference Method for Broth Dilution Antifungal Susceptibility Testing of Filamentous Fungi, second ed., CLSI, Wayne, PA, USA, 2008. Approved Standard M38-A2.
[27] M. Ocak, A. Helbok, C. Rangger, P.K. Peitl, B.A. Nock, G. Morelli, et al., Comparison of biological stability and metabolism of CCK2 receptor targeting peptides, a collaborative project under COST BM0607, Eur. J. Nucl. Med. Mol. Imag. 38 (2011) 1426–1435, https://doi.org/10.1007/s00259-011-1818-9.
[28] A. Skriba, T. Pluhacek, A. Palyzova, Z. Novy, K. Lemr, M. Hajduch, et al., Early and non-invasive diagnosis of aspergillosis revealed by infection kinetics monitored in a rat model, Front. Microbiol. 9 (2018) 1–7, https://doi.org/10.3389/fmicb.2018.02356.